Numerical prediction of cooling margins for a fluid with internal heat generation

A. Horvat [+], I. Kljenak [+] & J. Marn [*]
[+] *Reactor Engineering Division, "Jožef Stefan" Institute*
Ljubljana, Slovenia
[*] *Faculty of Mechanical Engineering, University of Maribor*
Maribor, Slovenia
E-mail: andrej.horvat@ijs.si

Abstract

Reactor pressure vessel lower plenum retention problem was studied to determine external cooling margins of the plenum walls. The accumulated melt was modelled as an incompressible fluid with internal volumetric heat generation in a rectangular cavity. A Smagorinsky type of Large-Eddy Simulation model for buoyancy flows was implemented. Because of uncertainty about upper wall thermal boundary conditions, isothermal and adiabatic boundary condition were used to assess heat transfer margins (Nusselt number) at each boundary of the simulation domain. It was found out in both calculated cases that the Nusselt number is the lowest at the bottom of the simulation domain and increases with height. In the future nuclear safety studies the most severe wall thermal conditions from both simulated cases will have to be considered.

1 Introduction

During a hypothetical accident scenario in the field of nuclear safety the general meltdown may occur as explained in Parzer [9]. The reactor core melts, relocates itself and accumulates in the lower plenum of the reactor vessel. Heat is further generated in the pool due to fission products decay. Because of high temperature melt, the integrity of the lower plenum could be threatened unless sufficient outside cooling exists. From an engineering point of view, the lower plenum retention problem is to determine the reliable external cooling margins of the plenum walls.

To do so, prediction of the fluid motion in a pool with internal heat generation is the crucial task. A review of experimental and theoretical results may be found, for example, in the work of Nourgaliev et al. [8].

At the present stage of knowledge, some uncertainties exist about heat removal from the surface of the pool which is exposed to the reactor core debris (Theofanous et al. [10]). Thermal conditions on the surface have a significant impact on the fluid dynamic behaviour of the pool. In the present work, the influence of two extreme thermal conditions (isothermal and adiabatic) at the pool upper surface on the fluid circulation was studied. At the other walls, isothermal conditions for temperature were prescribed to model melting and solidification processes.

2 Governing equations

In the present work the melt in the lower plenum is modelled considering an incompressible fluid with internal volumetric heat generation in a rectangular cavity. Using Boussinesq's approximation the equations of fluid motion are written as :

$$\nabla \cdot \vec{v} = 0 \quad , \tag{1}$$

$$\frac{\partial \vec{v}}{\partial t} + \nabla \cdot \left(\vec{v} \otimes \vec{v} \right) = -\frac{1}{\rho} \nabla p + \nabla \cdot \underline{\tau} - \beta \Delta T \, \vec{g} \quad , \tag{2}$$

$$\frac{\partial T}{\partial t} + \nabla \cdot \left(\vec{v} T \right) = \frac{\lambda}{c_p \rho} \nabla^2 T + \frac{I}{c_p \rho} \quad , \tag{3}$$

where v is the velocity, T is the temperature, p is the pressure modified for hydrostatic pressure, τ is the strain tensor, I is the rate of volumetric heat generation, g is the gravity acceleration, ρ is the density, β is the thermal dilatation, c_p is the specific heat and λ is the thermal conductivity.

The transformation of eqns (1), (2) and (3) into a dimensionless form as in Decker [2], simplifies the equations into :

$$\nabla \cdot \vec{v} = 0 \quad , \tag{4}$$

$$\frac{\partial \vec{v}}{\partial t} + \nabla \cdot \left(\vec{v} \otimes \vec{v} \right) = -\nabla p + \mathrm{Pr} \left(\nabla \cdot \underline{\tau} \right) - \mathrm{Ra}\,\mathrm{Pr}\, T \, \frac{\vec{g}}{|\vec{g}|} \quad , \tag{5}$$

$$\frac{\partial T}{\partial t} + \nabla \cdot \left(\vec{v} T \right) = \nabla^2 T + 1 \quad , \tag{6}$$

where Ra is the Rayleigh number and Pr is the Prandtl number.

The occurrence of hydrodynamic instabilities which leads toward turbulent fluid motion is correlated to the Rayleigh number. In our simulations, the Rayleigh number was 10^{10} and the Prandtl number 1.2, which was also the case in Nourgaliev et al. [8]. According to Decker [2], the transition to turbulent motion is expected already at $Ra \geq 5 \cdot 10^6$. For these reasons, proper turbulence model has to be implemented. In most cases, as it was summarized in Dinh et al. [3], standard or low Reynolds number *k-ε* models are used to model turbulent motion.

In the presented work, a Smagorinsky type of Large-Eddy Simulation model for buoyancy flows as developed in Eidson [4] and modified in Voke [12] was adopted. We were not successful in finding any previous implementation of a Large-Eddy Simulation model for turbulent natural convection flow with internal heat generation in open literature.

After using the Large-Eddy Simulation concept, eqns (4), (5) and (6) are written as :

$$\nabla \cdot \bar{\vec{v}} = 0 \quad , \tag{7}$$

$$\frac{\partial \bar{\vec{v}}}{\partial t} + \nabla \cdot (\bar{\vec{v}} \otimes \bar{\vec{v}}) = -\nabla \bar{p} + \mathrm{Pr}\left(\nabla^2 \bar{\vec{v}}\right) - \mathrm{Ra}\,\mathrm{Pr}\,\bar{T}\,\frac{\vec{g}}{|\vec{g}|} + \nabla \cdot \left(\nu_{sgd}\, 2\underline{\bar{S}}\right) \quad , \tag{8}$$

$$\frac{\partial \bar{T}}{\partial t} + \nabla \cdot \left(\bar{\vec{v}}\,\bar{T}\right) = \nabla^2 \bar{T} + 1 + \nabla \cdot \left(\upsilon_{sgd} \nabla \bar{T}\right) \quad , \tag{9}$$

where $^-$ denotes locally averaged values. The last terms in eqs (8) and (9) arise due to modelling of subgrid scale terms after filtering process. *S* is the deformation velocity tensor, ν_{sgd} is the subgrid viscosity defined as

$$\nu_{sgd} = \left(C_s \Delta x\right)^2 \left(2\underline{S} : \underline{S} + \frac{\mathrm{Ra}\,\mathrm{Pr}}{\mathrm{Pr}_{sgd}} \left(\nabla \bar{T} \cdot \frac{\vec{g}}{|\vec{g}|} \right) \right)^{1/2} \quad , \tag{10}$$

and υ_{sgd} is the subgrid thermal diffusivity defined as

$$\upsilon_{sgd} = \frac{\nu_{sgd}}{\mathrm{Pr}_{sgd}} \quad . \tag{11}$$

The Smagorinsky constant C_s and the turbulent Prandtl number $\mathrm{Pr}_{\mathrm{sgd}}$ are only empirical parameters in the presented turbulence model. In our case $C_s = 0.21$ and $\mathrm{Pr}_{\mathrm{sgd}} = 0.35$ as in Eidson [4].

As the Smagorinsky model is too dissipative in the vicinity of the walls, the use of turbulent viscosity damping functions is necessary. Madabhushi and Vanka [7] suggest the function (12) to damp excess subgrid viscosity as

$$f_d = \left(1 - \exp\left(-n^+/26\right)^3\right)^{1/2} \qquad (12)$$

,

where $n^+ = u_* n/\nu$ (u_* and n denote friction velocity and normal wall distance, respectively).

Eqns (7), (8) and (9) were solved applying no-slip boundary conditions at all boundary walls of a rectangular cavity. The boundary conditions for temperature were isothermal except at the top, where either isothermal or adiabatic boundary conditions were prescribed.

3 Numerical methods

Time dependent transport eqns (7), (8) and (9) with appropriate boundary conditions were solved using a two-dimensional numerical code based on the finite volume method as described in Versteeg and Malalasekera [11].

For spatial discretisation a staggered grid was implemented. Numerical discretisation of momentum eqn (8) followed the way of the Harlow and Walsh [5] scheme. However, the temperature field in the energy eqn (9) required a 2nd order accurate upwind scheme.

Time integration was independent from spatial discretization. For energy eqn (9) the 2nd order accurate Adam-Bashford scheme was implemented :

$$\frac{\overline{T}^{n+1} - \overline{T}^{n}}{\Delta t^n} = RHS^{n+1/2} \ , \qquad (13)$$

$$RHS^{n+1/2} = RHS^{n} + 0.5\Delta t^n \frac{\left(RHS^n - RHS^{n-1}\right)}{\Delta t^{n-1}} \ . \qquad (14)$$

In the case of momentum eqn (8) a combination of Adam-Bashford scheme and projection method was used.

In this way, the solenoid velocity field $\vec{\overline{v}}$ is uniquely decomposed into velocity field $\vec{\overline{v}}^*$, which is not divergence free, and gradient of pressure p as it is extensively described in Bell et al. [1]. Consequently, the decomposition leads to the following steps in the time integration procedure of momentum eqn (8). First, the auxiliary vector field $\vec{\overline{v}}^*$ is

computed from equation (15) :

$$\vec{\bar{v}}^{*} = \Delta t \left(RHS^{n+1/2} \right) + \vec{\bar{v}}^{n} \quad . \tag{15}$$

Then, the pressure field is calculated using mass conservation equation (7) in order to obtain the Poisson equation $\nabla^2 p = \nabla \vec{\bar{v}}^{*} / \Delta t$. In our case the Poisson equation was solved implementing a direct Poisson solver. At the end the gradient of pressure field p is added :

$$\vec{\bar{v}}^{n+1} = -\Delta t \left(\nabla \bar{p} \right) + \vec{\bar{v}}^{*} \quad . \tag{16}$$

In the presented work 128x128 grid points were used to perform calculations. Approximately 60 hours of CPU time on Sun Ultra 2 workstation were necessary to reach steady-state conditions.

4 Results and discussion

Numerical simulations were performed at Rayleigh number 10^{10} and Prandtl number 1.2, which is a well documented case and corresponds to the thermal situation in the reactor vessel lower plenum. To validate the numerical code simulation results were compared with the results of Nourgaliev et al. [8].

For the case of isothermal upper boundary the integral Nusselt numbers for each boundary were calculated. Comparison of results is presented in table 1. It shows good agreement with some discrepancies in case of upper boundary due to thermal instabilities.

Table 1: Comparison of results for isothermal upper boundary .

boundary	*present calculations*	*Nourgaliev et al.* [8]
bottom	Nu = 14.815	Nu = 14.535
side	Nu = 67.646	Nu = 66.480
upper	Nu = 90.940	Nu = 73.184

The distribution of heat transfer at the bottom wall was also calculated. Fig 1 shows the comparison between present calculations and calculations made by Nourgaliev et al. [8]. Again the results are in good agreement with those already published (Nourgaliev et al. [8]) .

These comparisons were done to demonstrate the capability of the described approach to model turbulent natural convection in fluids with internal heat generation as discussed also in Horvat and Kljenak [6]

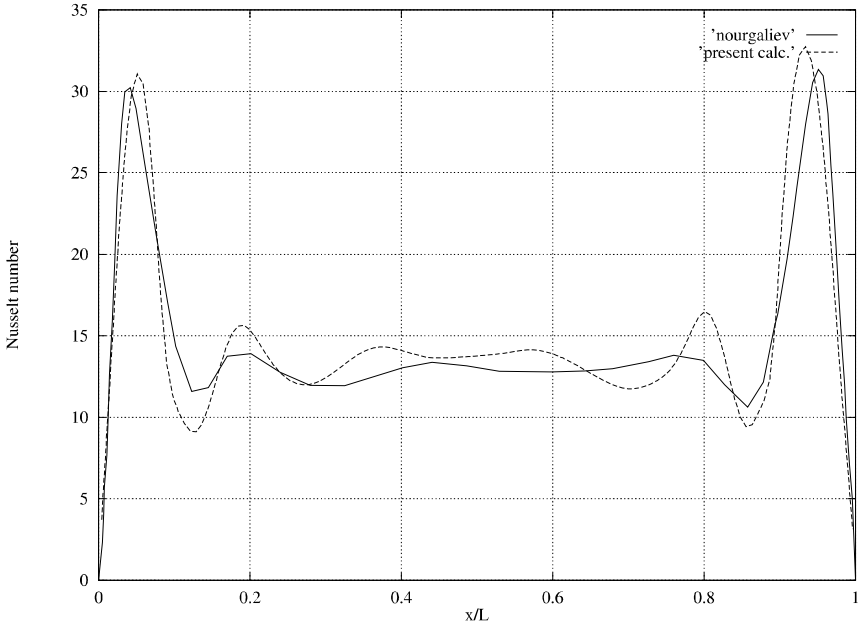

Figure 1: Nusselt number at bottom boundary of simulation domain.

Because of uncertainty about upper wall thermal boundary conditions, the isothermal and adiabatic boundary conditions were used to assess heat transfer margins (cooling margins) at each boundary of the simulation domain. On fig 2 the cooling margins on bottom and side walls for the case of upper wall isothermal and adiabatic boundary conditions are presented.

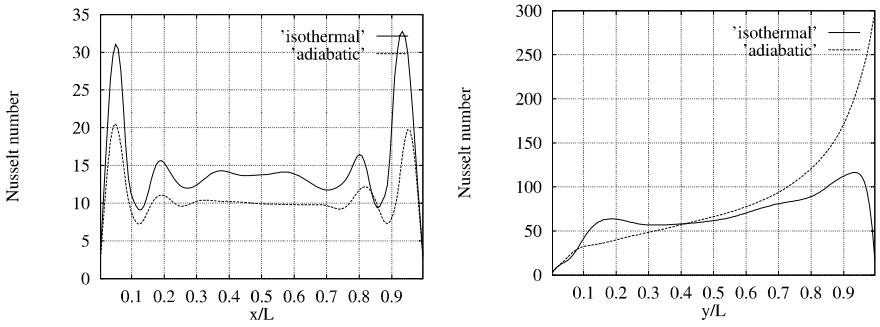

Figure 2: Local Nusselt number at bottom (left) and side (right) walls .

Cooling margins on upper wall for the case of upper wall isothermal and adiabatic boundary conditions are presented on fig 3.

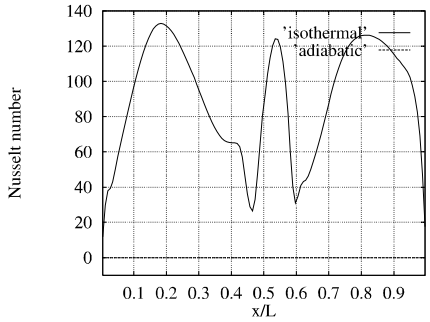

Figure 3: Local Nusselt number at upper wall .

It was found out in both calculated cases that the Nusselt number is the lowest at the bottom of the simulation domain and increases with height. In the case of upper wall isothermal boundary conditions the heat transfer is increased through the bottom and reduced through the side walls whereas in the case of upper wall adiabatic boundary conditions the heat transfer is increased through the side walls and reduced through the bottom. The largest heat transfer can be expected in the case of upper wall adiabatic boundary conditions in the vicinity of the upper boundary, where it reaches a local value of Nu = 300.

Fig 4 shows qualitative velocity vector fields for upper wall isothermal and adiabatic boundary conditions.

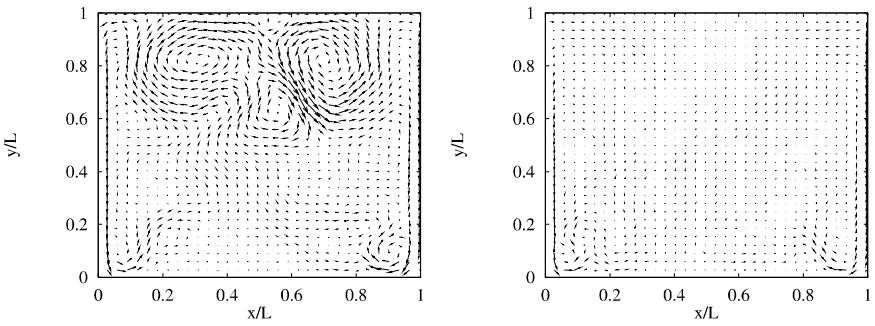

Figure 4: Qualitative velocity vector field for upper wall isothermal (left) and adiabatic (right) boundary conditions.

It can be observed on fig 4 that velocities are greater in the case of upper wall isothermal boundary conditions. At the upper wall the fluid is cooled and the intrusions of cold streams stretch deep into the bulk. In the case of upper wall adiabatic boundary conditions the velocity field is more stable and the intrusions of cold streams are not present.

On fig 5 the temperature fields for upper wall isothermal and adiabatic boundary conditions are presented with isotherms. The dimensionless temperature is between 0.0 to 0.015 with distances of 0.001 between isotherms.

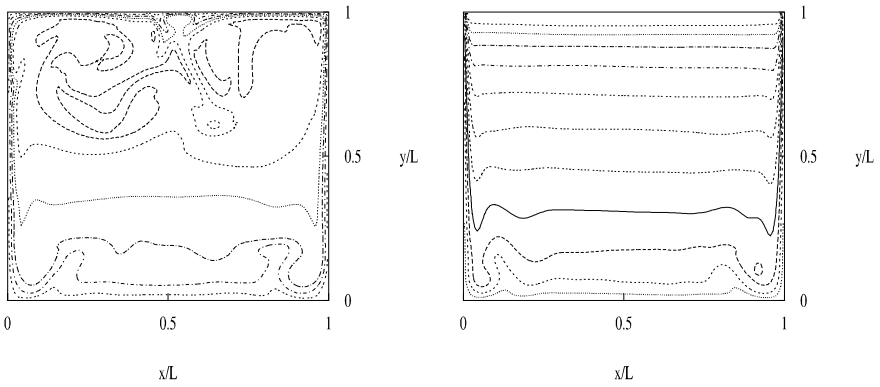

Figure 5: Temperature field for upper wall isothermal (left) and adiabatic (right) boundary conditions.

Fig 5 (right) shows stable stratification of temperature field with increasing temperature from bottom to top in the case of upper wall adiabatic boundary conditions. In the case of upper wall isothermal boundary conditions (left) only the lower part of the melt pool is stratified. The upper part of the temperature field is influenced by intrusions of cold streams.

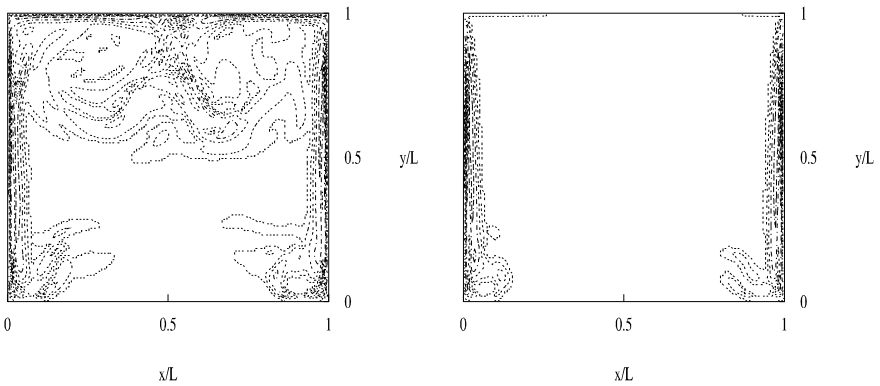

Figure 6: Turbulent viscosity field for upper wall isothermal (left) and adiabatic (right) boundary conditions.

This phenomena can be also seen on fig 6, which shows turbulent viscosity fields for upper wall isothermal (left) and adiabatic (right) boundary conditions with isolines. The dimensionless turbulent viscosity is between 0.0 and 0.4 with distances of 0.05 between isolines.

The turbulent viscosity is modestly developed in the case of adiabatic boundary conditions. On the contrary, in the case of isothermal boundary conditions the higher velocities and intrusions of cold streams from the upper wall boundary layer produce locally strong turbulence.

5 Conclusions

The influences of thermal conditions on the surface of melt pool in lower plenum were studied to investigate upper limits of heat transfer through the plenum's wall.

The melt was modelled as a fluid with internal heat generation at Rayleigh number $Ra = 10^{10}$ and Prandtl number $Pr = 1.2$. The thermal boundary conditions were isothermal at the bottom and side walls. At the top, adiabatic and isothermal boundary conditions were used to assess heat transfer bounds.

The modified Smagorinsky subgrid model was used to model turbulent behaviour of the fluid. We were not successful in finding any previous implementation of a Large-Eddy Simulation model for turbulent natural convection flow with internal heat generation in open literature.

Results obtained with numerical integration show that upper wall adiabatic boundary conditions reduce heat transfer through the bottom wall and increase it through the side walls. We also calculated the largest heat transfer which occurs in the case of upper wall adiabatic boundary conditions in the vicinity of top boundary.

Because of difficulties predicting the exact thermal conditions on the pool surface during a specific meltdown scenario, the future nuclear safety studies will have to consider most severe wall thermal conditions from both simulated cases.

In the future work the flows with higher Rayleigh number will be modelled using the presented approach.

References

[1] Bell, J. B., Colella, P. & Glaz, H. M., 1989, A Second Order Projection Method for the Incompressible Navier-Stokes Equation, *J. Comp. Phys* , **2**, pp. 257-283, 1989.

[2] Decker, W. J., *Numerical Studies of Bifurcations and Chaos in Natural Convection*, Ph. D. Thesis, University of Virginia, 1996.

[3] Dinh, T. N. & Nourgaliev, R. R., Turbulence Modelling for Large Volumetrically Heated Liquid Pools, *Nucl. Eng. Design*, **169**, pp. 131-150, 1997.

[4] Eidson, T., Numerical Simulation of the Turbulent Rayleigh-Bénard Problem using Subgrid Modelling, *J. Fluid. Mech*., **158**, pp. 245-268, 1985.

[5] Harlow, F. H. & Welch, J. E., Numerical Calculation of Time-Dependent Viscous Incompressible Flow of Fluid with Free Surface, *Phys. Fluids*, **12**, pp. 2182-2186, 1965.

[6] Horvat, A., Kljenak, I., Numerical Investigation of Turbulent Natural Convection in Reactor Pressure Vessel Lower Plenum during Core Meltdown Scenario, *Proc. of the 4th Regional Meeting: Nuclear Energy in Central Europe*, eds. B. Mavko & L. Cizelj, Nuclear Society of Slovenia, Ljubljana, pp. 43-50.

[7] Madabhushi, R. K. & Vanka, S. P., Large-Eddy Simulation of Turbulence-Driven Secondary Flow in a Square Duct, *Phys. Fluids A*, **11**, pp.2734-2745, 1991.

[8] Nourgaliev, R. R., Dinh, T. N. & Sengal, B. R., Effect of Fluid Prandtl Number on Heat Transfer Characteristics in Internally Heated Liquid Pools with Rayleigh Numbers up to 10^{12} , *Nucl. Eng. Design*, **169**, pp. 165-184, 1997.

[9] Parzer, I., Phenomena during a LB Loca Accident Predicted by MELCOR Code, *Proc. of the 3rd Regional Meeting: Nuclear Energy in Central Europe*, eds. A. Stritar & I. Jenčič, Nuclear Society of Slovenia, Ljubljana, pp. 221-228.

[10] Theofanous, T. G., Liu, C., Addition, S., Angelini, S., Kymäläinen, O. Salmassi, T., In-vessel Coolability and Retention of a Core Melt, *Nucl. Eng. Design*, **169**, pp. 1- 48, 1997.

[11] Versteeg, H. K. & Malalasekera, W., *An Introduction to Computational Fluid Dynamics, The Finite Volume Method*, Longman Scientific & Technical, England, pp. 103-133 ,1995.

[12] Voke, P., Low-Reynolds-Number Subgrid-Scale Models, *Theoret. Comput. Fluid Dynamics*, **2**, 1996.